NON-RESONANT MULTIPACTOR MECHANISM AND SEY IMPACT IN A VHF CW ELECTRON GUN*

Yitong Duan, Lianmin Zheng†, Yingchao Du
Department of Engineering Physics, Tsinghua University, Beijing, China and
Key Laboratory of Particle and Radiation Imaging, Tsinghua University,
Ministry of Education, Beijing, China

Abstract

Electron trajectory analysis within the cavity shows that the energy dispersion and angular distribution of secondary electrons strongly influence their dynamic behavior. Despite the overall non-resonant nature of multipactor, multiple resonant modes can still be identified from the statistical distribution of electron flight times. This work investigates the effect of RF cavity geometry on multipactor characteristics, and clarifies the underlying mechanisms via statistical analysis of particle trajectories.

INTRODUCTION

Multipactor [1] is a nonlinear electron multiplication phenomenon induced by high-frequency electromagnetic fields in radio-frequency (rf) devices under vacuum. When primary electrons, accelerated by these electromagnetic fields, impinge on metallic or dielectric surfaces,they generate secondary electrons that further strike the surfaces, triggering an electron avalanche through continuous multiplication. In particle accelerators, multipactor is most likely to occur in resonant cavities operating in long-pulse or continuous-wave (CW) modes. CW resonant cavities are especially prone to this phenomenon, as continuous microwave excitation facilitates the rapid accumulation of secondary electrons.

The very-high-frequency (VHF) photocathode electron gun [2] is a typical resonant cavity working in CW mode. In this study, we verify that the multipactor occurring within the cavity is non-resonant [3], meaning that the motion of electrons is not synchronized with the time-varying electromagnetic field.

SIMULATION SETUP

The Furman model [4] is rooted in a rigorous physical foundation and functions as a phenomenological probabilistic framework. It quantifies the stochasticity of electron–surface collisions by linking microscopic event probabilities to macroscopic measurable parameters. In this model, each electron–surface collision generates n secondary electrons ($n = 0, 1, 2, \ldots$), where P_n denotes the probability of emitting exactly n secondary electrons. For physical consistency, the probabilities satisfy the normalization condition, with P_0 representing the absorption probability of incident electrons (no secondary emission):

$$\sum_{n=0}^{\infty} P_n = 1, \quad P_n \geq 0. \tag{1}$$

The secondary electron yield (SEY) δ is the expectation of secondary electron number n, defined as:

$$\delta = \langle n \rangle = \sum_{n=1}^{\infty} n P_n. \tag{2}$$

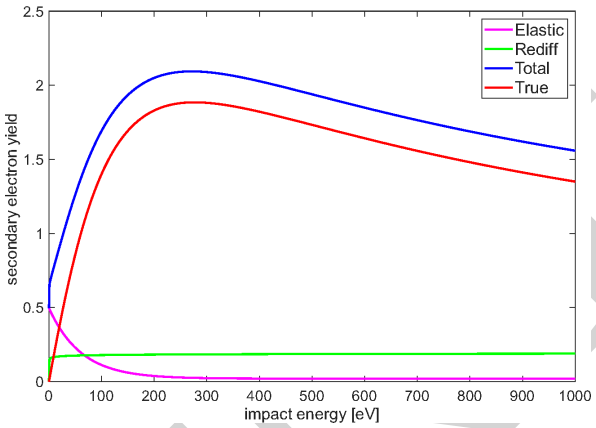

Figure 1: SEY of copper as a function of incident electron energy in CST Furman model.

The Furman model divides secondary electron yield (SEY) into three components: true secondary, rediffused, and elastically backscattered electrons, which correspond to three distinct physical emission mechanisms. Measured secondary electron yield (SEY) values vary considerably among different research groups, mainly attributed to differences in copper impurity content and surface treatment techniques. To guarantee the conservativeness of simulations, we adopted the Furman model embedded in CST, as illustrated in Fig. 1.

NON-RESONANT MULTIPACTOR

Previously, multipactor intensity was evaluated by tracking the evolution of particle count. Here, we analyze microscopic electron trajectories to reveal multipactor behavior from the perspective of electron dynamics. Typical trajectories of primary and secondary electrons are shown in Fig. 2.

Under time-varying electromagnetic fields, the primary electron experiences repeated acceleration and deceleration with significant deflection, reaching a peak energy of 400 eV

* Work supported by the National Natural Science Foundation of China (NSFC) under Grant No. 12275149.
† zhenglm2019@mail.tsinghua.edu.cn

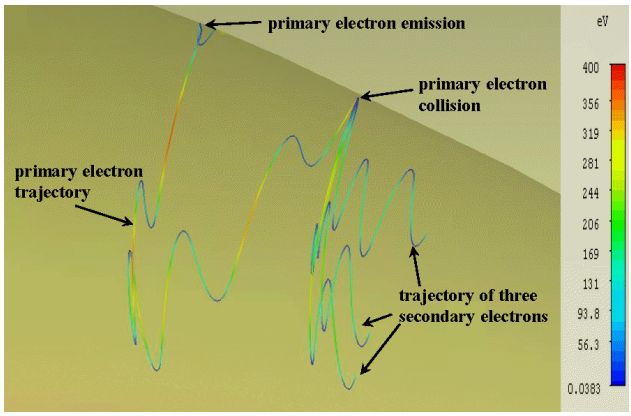

Figure 2: Typical trajectories of primary and secondary electrons in CST.

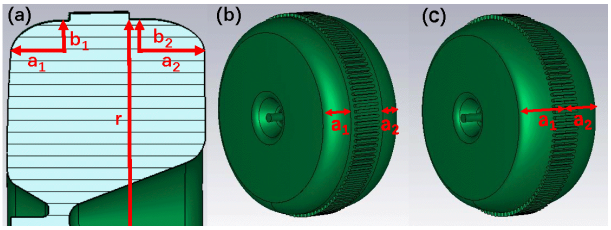

Figure 3: (a) Gun cavity profile with critical geometric parameters. (b) and (c) present multipacting-optimized cavity configurations: (b) baseline design retaining a linear segment between elliptical corners; (c) proposed equatorial geometry with maximized elliptical major axes.

and dropping below 1 eV at minimum.Its trajectory extends over several microwave cycles before impacting the cavity wall and generating secondary electrons.

According to Furman's probabilistic model, the number of emitted secondaries is stochastic; in the figure, three secondary electrons are produced with small differences in initial energy and emission angle. Due to the weak electric field near the emission point and long flight duration, their trajectories diverge strongly, leading to distinct impact positions on the cavity surface. This regime corresponds to non-resonant multipactor. Unlike one-surface and two-surface resonant multipactors, which can be well modeled analytically, non-resonant multipactor is difficult to analyze, particularly in complex curved structures such as VHF electron guns. Therefore, full-particle dynamics simulations in CST offer an effective and practical approach to studying non-resonant multipactor.

MULTIPACTOR MECHANISM ANALYSIS

Figure 3 (a) defines key geometric parameters governing multipactor strength: cavity radius r, major axes (a_1, a_2), and minor axes (b_1, b_2) of the elliptical corners. Conventional designs preserve a linear segment between elliptical corners (Fig. 3 (b)), whereas the proposed equatorial cavity geometry (Fig. 3 (c)) removes this segment while maximizing the elliptical major axes.

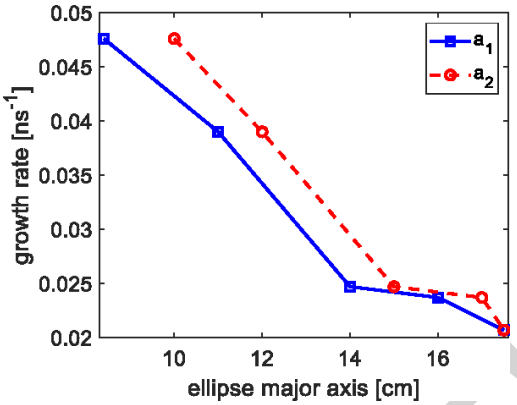

Figure 4: Dependence of secondary electron growth rate α on elliptical major axes under a 7 MV/m cathode gradient.

Initial parameters were fixed as: cavity radius $r = 34.7$ cm, elliptical minor axes $b_1 = b_2 = 5.7$ cm, and cathode-anode gap = 3.5 cm. The elliptical major axes a_1 and a_2 were increased to 17.5 cm for full ellipse contact, with other cavity dimensions optimized in CST Microwave Studio to maximize RF performance. Multipactor intensity was then evaluated via the growth rate α in CST Particle Studio.Figure 4 shows that α decreases significantly with increasing elliptical major axes at 7 MV/m.

For resonant multipactor, the secondary electron growth rate α mainly depends on electron flight time T and secondary electron yield (SEY) δ. Substituting T and δ into the equation gives:

$$N_e(T) = N_0 e^{\alpha T} = N_0 \delta \tag{3}$$

$$\alpha = \frac{\ln \delta}{T} \tag{4}$$

For non-resonant multipactor, Eq. (4) is not strictly valid, but its qualitative trend holds: a large multipactor intensity parameter α corresponds to a small average secondary electron flight time $\bar{T}$ and a large SEY δ, where $\bar{T}$ is the average flight time of all secondary electrons.

The flight time distributions of secondary electrons for two cavity geometries are statistically analyzed in Fig. 5, based on 15,000 particles tracked under stable multipactor conditions. The rf period is $T_{\mathrm{rf}} = 4.62$ ns. Both structures show a large number of electrons with flight times below 1.2 ns, typical of non-resonant multipactor. Distinct peaks appear at integer multiples of T_{rf} up to the fifth order (4.62 ns, 9.23 ns, 13.85 ns, 18.46 ns, 23.08 ns), indicating multiple resonant modes. The equatorial cavity ($a_1 = a_2 = 17.5$ cm) exhibits all five orders, while the non-contacting geometry ($a_1 = 8.4$ cm, $a_2 = 10$ cm) shows only the first three. The average flight times are $\bar{T} = 7.93$ ns and 8.12 ns, respectively.

The probability distribution P_n of secondary electrons per impact is shown in Fig. 6. The non-contacting cavity has a significantly higher probability of emitting more than two secondary electrons per collision. Using Eq. 2, the corresponding SEY values are $\delta = 1.6112$ and $\delta = 1.2285$, respectively.

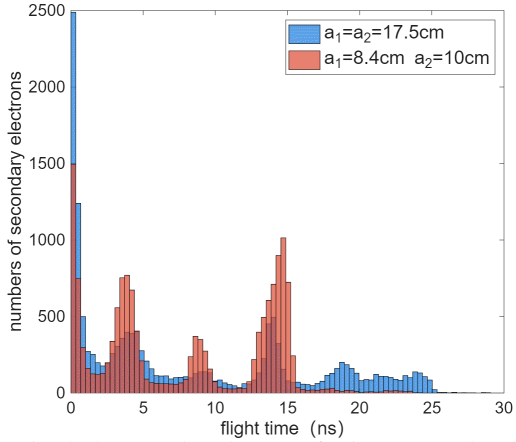

Figure 5: Flight time distribution of 15,000 particles during stable multipacting for two cavity shapes.

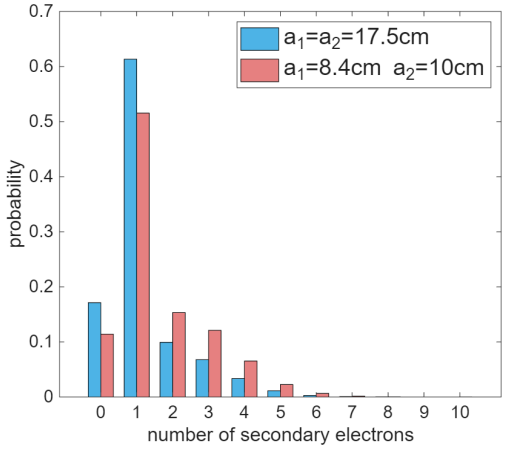

Figure 6: Probability distribution P_n of secondary electron yield per electron impact for two cavity shapes.

In summary, the equatorial cavity has a longer average flight time and lower SEY, leading to a weaker multipactor strength α according to Eq. 4.

As shown in Fig. 1, the secondary electron yield (SEY) strongly depends on the primary electron impact energy. To explain the lower SEY in the equatorial cavity, we quantify the impact energy. Under stable multipacting conditions, the impact energy distributions of 15,000 particles for both cavity shapes are presented in Fig. 7. The impact energy in the equatorial cavity is mainly below 100 eV, whereas the non-contacting cavity (a_1 = 8.4 cm, a_2 = 10 cm) has a peak near 250 eV. As verified in Fig. 1, 250 eV corresponds to the maximum SEY in the CST Furman model. Therefore, Fig. 7 provides an intuitive explanation for the low δ in the equatorial cavity from the perspective of impact energy statistics.

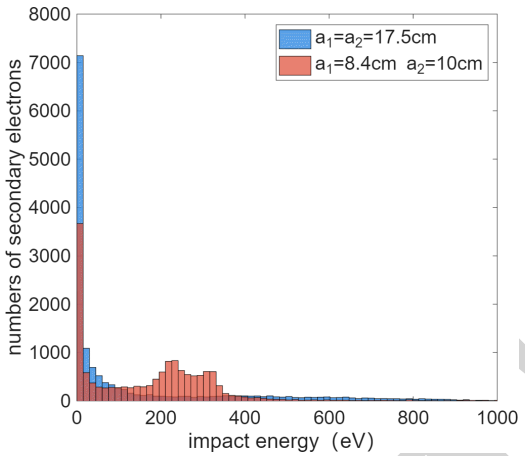

Figure 7: Impact energy distribution of 15,000 particles during stable multipacting state for two cavity shapes.

CONCLUSION

In this work, electron trajectory analysis shows that the cavity multipactor is non-resonant, with electron motion out of synchronism with the RF field. The energy and angular spread of emitted secondary electrons disturbs the resonance condition and strongly affects electron dynamics. Although dominated by non-resonant behavior, multiple resonant modes can still be identified from flight-time statistics. Based on statistical analysis of flight time, emission probability, and impact energy, we clarify how cavity geometry modification suppresses multipactor intensity.

REFERENCES

[1] A. Iqbal, D.-Q. Wen, J. Verboncoeur, and P. Zhang, "Recent advances in multipactor physics and mitigation", *High Voltage*, vol. 8, no. 6, pp. 1095–1114, 2023. doi:10.1049/hve2.12335

[2] L. Zheng *et al.*, "Design, fabrication, and beam commissioning of a 216.667 MHz continuous-wave photocathode very-high-frequency electron gun", *Physical Review Accelerators and Beams*, vol. 26, no. 10, p. 103402, 2023. doi:10.1103/PhysRevAccelBeams.26.103402

[3] J. Rasch and J. Johansson, "Non-resonant multipactor—a statistical model", *Physics of Plasmas*, vol. 19, no. 12, 2012. doi:10.1063/1.4771675

[4] M. Furman and M. Pivi, "Probabilistic model for the simulation of secondary electron emission", *Physical Review Special Topics—Accelerators and Beams*, vol. 5, no. 12, p. 124404, 2002. doi:10.1103/PhysRevSTAB.5.124404